CPG-based Motion Planning of Hybrid Underwater Hexapod Robot for Wall Climbing and Transition

Feiyu Ma, Weisheng Yan, Lepeng Chen and Rongxin Cui

***Abstract*—Most of the existing underwater legged robots are capable of moving on small-angled slopes, but few of them can climb the large-angled slope or transition from one plane to another, such as transition from horizontal plane to vertical plane. In this paper, we propose a motion planning method of a hybrid underwater hexapod robot (HUHR) driven by six C-shape legs and eight thrusters. By analyzing the relationship between rotation and displacement of the hip joint, we establish a single-leg kinematic model. By analyzing the force at the touchpoint, we propose a locomotion mechanism to ensure no slip of the C-shape leg. Based on the central pattern generator (CPG) and tripod gait, we design an aperiodic mapping between the oscillator outputs and the desired rotation angles of hip joints. Overall, a gait planning and control method for our robot is proposed to realize continuous legged locomotion from one plane to another, including directional climbing and transition between them. Furthermore, the effectiveness of the proposed method has been verified on HUHR.**

***Index Terms*—Hybrid underwater hexapod robot, Legged locomotion, Central pattern generator, Climbing and transition.**

I. Introduction

A. Background

NOWADAYS, Unmanned Underwater Vehicles (UUVs) play an important role in hazardous operations, such as ocean exploration, and maritime search and rescue. UUVs are mainly divided into Remotely Operated Vehicles (ROVs) and Autonomous Underwater Vehicles (AUVs), both of them driven by thrusters to carry out different missions. However, due to the ability to land, adhere, and climb on complex operating surfaces, walking robots are more suitable to perform some refined operations than traditional UUVs, such as the cleaning of ships, daily maintenance of oil rigs, and safety inspection of reservoir dams. Therefore, developing an underwater robot with both cruising and walking capabilities is significant. In this paper, different from traditional UUVs, we introduce a new hybrid underwater hexapod robot, called HUHR, driven by thrusters and C-shape legs, as shown in Fig. 1, equipped with Inertial Measurement Unit (IMU) and Joint Angle Encoder. The accuracy of IMU is $\pm 0.05^\circ$ RMS (Pitch, Roll), $\pm 1^\circ$ RMS (Yaw). The resolution of Joint Angle Encoder is 0.01°. This robot combines the cruising capability of UUVs and the walking capability of legged robots. It has six C-shape legs that combine the maneuverability of a wheeled leg with the obstacle climbing ability of a crab leg, and each leg only has one degree of freedom for easy control. Moreover, the rolling contact is more effective than the point contact for the legged robot [1], and the C-shape leg can adapt to a variety of terrains with its stronger mobility [2]–[4]. However, in order to ensure no slip of HUHR, designing coordinating control inputs of thrusters and legs is essential and difficult.

(a) (b)

Fig. 1. The hybrid underwater hexapod robot. (a) The experiment platform. (b) The 3D model of HUHR.

Due to the hybrid drive, HUHR owns many motion modes, including cruising, walking and climbing, as shown in Fig. 2, where $\bar{\theta}^{(k)}(k = 1, 2)$ is the angle between the kth plane and the horizontal plane, which we call the pitch angle of the kth plane. When HUHR needs to switch from cruising to climbing, we can adjust its attitude with thrusters directly so that HUHR can adhere to the wall and start climbing. However, when HUHR needs to switch between walking and climbing, which can be seen as a transition between planes with different pitch angles, called the transition phase in this paper, it's more convenient to switch by legs directly. Staying adhered to the wall, instead of floating, HUHR has a landing point, which

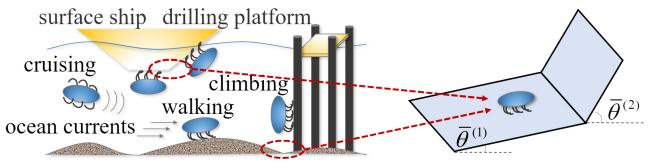

Fig. 2. The motion modes of HUHR.

Manuscript received: June 10, 2022; Revised: September 2, 2022; Accepted: October 10, 2022. This paper was recommended for publication by Editor Pauline Pounds upon evaluation of the Associate Editor and Reviewers'comments. This work was supported by the National Natural Science Foundation of China(NSFC) under grant 61733014, grant U1813225 and grant U21B2047, and by the Key Research and Development Program of Shaanxi under grant 2020ZDLGY06-07. (*Corresponding author: Weisheng Yan, Rongxin Cui.*)

The authors are with School of Marine Science and Technology, Northwestern Polytechnical University, Xi'an 710072, China. mfy_nwpu@mail.nwpu.edu.cn; wsyan@nwpu.edu.cn; chenlepeng@mail.nwpu.edu.cn; r.cui@nwpu.edu.cn

Digital Object Identifier (DOI): see top of this page.

can resist ocean current disturbance more effectively and is less prone to moving sideways. Therefore, designing a gait planning method for HUHR to perform smooth transitions is both practical and challenging.

B. Related Work

Legged locomotion methods can be mainly classified into model-based methods and bionics-based methods. In [5], a rolling spring-loaded inverted pendulum model for the RHex robot was proposed to realize jumping motion. In [6], a data-driven modeling method for the X-Rhex robot was proposed. However, model-based methods are often complex and prone to model errors, several researchers have turned to bionic-based method for gait planning, such as central pattern generator (CPG) [7], which is simple to model and easy to implement. In [8], a gait planning method for the amphibious robot was implemented based on the Hopf oscillator. In [9]–[11], CPG motion control networks were built respectively, that achieved legged locomotion for hexapod robots. However, those existing CPG-based methods all generate periodic gait, which cannot realize the transition between different walls, especially the transition between horizontal planes and vertical planes. So we proposed an aperiodic gait based on CPG in this paper.

Furthermore, for existing underwater wall-climbing robots, most studies focus on climbing rather than transitioning, which severely limits their motion capabilities [12]–[14]. Unlike existing studies, we focus on the problem of smooth transition in this paper, and provide a transition strategy for HUHR. Due to the lack of research about underwater walking robots, by taking land robots as examples, we introduce some existing transition strategies. For example, in [15]–[18], the soft robots can bend freely to transition between different walls, which is clearly not suitable for our rigid robot. Moreover, for rigid robots, existing transition strategies were mostly achieved by adding stabilization modules [19]–[21] or designing the robot into a multi-linked and variable structure to achieve the transition [22], [23]. However, the HUHR is not deformable, so we achieve the transition strategy only by designing a reasonable gait and suitable control inputs for thrusters. What's more, unlike the method in [24], which can only realize the transition from a horizontal plane to a slope within 20°, our method allows HUHR to transition from the horizontal to the vertical plane.

C. Contribution

To realize continuous legged locomotion, such as transitioning from horizontal planes to vertical planes, we propose a gait planning and control method for HUHR. The difficulties of continuous legged locomotion lie in three aspects: the design of aperiodic gait, the coordination of two driving modes, and the adaptivity of the method.

Firstly, existing CPG-based gait planning methods are periodic, which means they cannot adapt to the change in the walking plane. We need to find an aperiodic gait to satisfy the kinematic constraints during transition phase for our robot. Secondly, because our robot is hybrid driven, the difficulty lies in the dynamic constraint of the robot, which should ensure the legs do not slip and overload. Thirdly, the control inputs should be self-regulating when the robot climbing different planes.

The main contributions can be specified as follows.

(1) The stable walking constraints of HUHR are analyzed, and the motion mechanism of the robot that make sure the C-shape leg do not slip is revealed.

(2) An aperiodic mapping relationship from the output of Hopf oscillator to the rotation angle of the hip joint was designed, and a CPG-based gait planning method is proposed.

(3) Considering the restoring forces and restoring moments of HUHR, a directional climbing gait planning and control method is designed, which adapt to different walls.

II. Preliminaries and Problem Formulation

A. Coordinate System and Parameter Definition

The coordinate systems involved in this paper are shown in Fig. 3, where $O_0X_0Y_0Z_0$, $O_bX_bY_bZ_b$, $O_{hi}X_{hi}Y_{hi}Z_{hi}$ and $O_{pi}X_{pi}Y_{pi}Z_{pi}$ represent the earth-fixed coordinate system, the body-fixed coordinate system, the hip joint coordinate system and the touchpoint coordinate system, respectively.

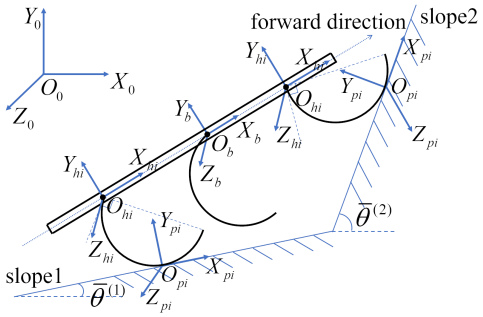

Fig. 3. Coordinate system diagram.

HUHR is driven by six C-shape legs and eight thrusters, four of them are vertical thrusters ($T_1 - T_4$) and others are lateral thrusters ($T_5 - T_8$). The placement of thrusters and hip joints of C-shape legs is shown in Fig. 4, where $d_m(m = 1, 2)$ and $l_n(n = 1, 2, 3, 4)$ represent the distance between the thrusters and hip joints, respectively. The arrow in Fig. 4(b) points in the direction of the thrust generated by the positive rotation of the thruster.

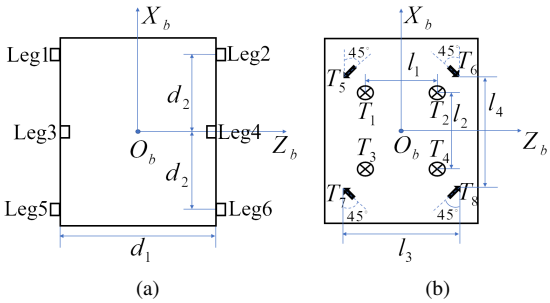

Fig. 4. The placement of thrusters and hip joints. (a) Six hip joints of C-shape legs. (b) Eight thrusters.

According to the placement of thrusters shown in Fig. 4(b), the thrust distribution matrix $\mathbf{C}_T$ can be described as

$$\mathbf{C}_T = \begin{bmatrix} 0 & 0 & 0 & 0 & -\frac{\sqrt{2}}{2} & -\frac{\sqrt{2}}{2} & \frac{\sqrt{2}}{2} & \frac{\sqrt{2}}{2} \\ -1 & -1 & -1 & -1 & 0 & 0 & 0 & 0 \\ 0 & 0 & 0 & 0 & -\frac{\sqrt{2}}{2} & \frac{\sqrt{2}}{2} & -\frac{\sqrt{2}}{2} & \frac{\sqrt{2}}{2} \\ -\frac{l_1}{2} & \frac{l_1}{2} & -\frac{l_1}{2} & \frac{l_1}{2} & 0 & 0 & 0 & 0 \\ 0 & 0 & 0 & 0 & l & -l & -l & l \\ -\frac{l_2}{2} & -\frac{l_2}{2} & \frac{l_2}{2} & \frac{l_2}{2} & 0 & 0 & 0 & 0 \end{bmatrix} \tag{1}$$

where $l = \frac{\sqrt{2}}{2}\left(\frac{l_3}{2} + \frac{l_4}{2}\right)$.

B. Single-leg Kinematic Model

Assuming that the C-shape leg of HUHR is rigid, the connection between the hip joint and the touchpoint can be equivalent to a rigid connecting rod, whose length varies with the rotation angle of hip joint. Single-leg movement can be divided into two parts: rolling along the wall and swinging in the water, which correspond to the supporting phase and the swinging phase, respectively. The gait-related terms are defined in TABLE I.

Symbol	Meaning
θ_s	The angle at which hip joint is turned in the supporting phase
θ_t	The angle at which hip joint is turned in the swinging phase
θ_c	The angle of hip joint when the C-shape leg is about to touch the wall
θ_f	The angle of hip joint when the C-shape leg is about to leave the wall
T	The total time required for supporting phase and swinging phase
ε	The ratio of duration of the supporting phase to T

TABLE I
THE GAIT-RELATED TERMS

Fig. 5 shows the motion diagram of a single C-shape leg, where S represents the hip joint of HUHR, O/O' represents the center of the circle which includes the C-shape leg, and $P/Q/M$ represents the touchpoint of C-shape leg. $q_i\,(i = 1, \cdots, 6)$ is the rotation angle of the ith hip joint, which is defined as the angle between the positive direction of the O_bX_b axis and the tangent line of the C-shape leg at the hip joint. $\theta_{si}\,(i = 1, \cdots, 6)$ is the support angle of the ith C-shape leg, "position1" and "position2" show the placement of the hip joint when the leg is about to touch and leave the wall, respectively. During the movement of HUHR, in order to reduce the fluctuation of the robot along the direction of the O_0Y_0 and the pitch angle of the robot, the position1 and the position2 should be set as axial symmetry about O_bY_b. At this point, when $q = \pi$ (position3), as shown in Fig. 5, SM is perpendicular to the wall, as well as SA and SQ are symmetric about SM.

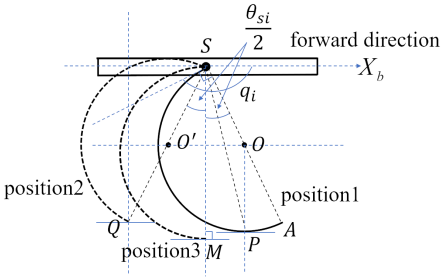

Fig. 5. The movement of the C-shape leg.

During the whole movement, the displacement of the hip joint in the $O_{pi}X_{pi}$ axis and $O_{pi}Y_{pi}$ axis can be described as

$$\begin{cases} l_x = \left(\dfrac{\theta_{si}}{2} + 3\sin\dfrac{\theta_{si}}{2}\right) l_r \\ l_y = 2l_r\left(1 - \cos\dfrac{\theta_{si}}{2}\right) \end{cases} \tag{2}$$

where l_r is the radius of the C-shape leg, l_x and l_y are the distance that the hip joint moves along the O_pX_p axis and O_pY_p axis, respectively. The variation of l_y is very small, when $\theta_{si} = \frac{\pi}{3}$rad, l_y only varies by 2.3 cm, so the robot's vertical movement from the leg motion are ignored in this paper.

C. Stable Walking Constraint

When the robot moves, basic thrust $T_i^b\,(i = 1, 2, \cdots, 8)$ should ensure the C-shape legs do not slip. The force analysis at the touchpoint of each leg is shown in Fig. 6, where S_i denotes the ith hip joint of the robot, O_i is the circular position of the ith leg, P_i indicates the touchpoint of the ith leg, θ is the pitch angle of the robot, τ_i is the joint torque of the ith leg, N_i and f_i are the support forces and friction forces provided by the wall at the ith touchpoint, respectively.

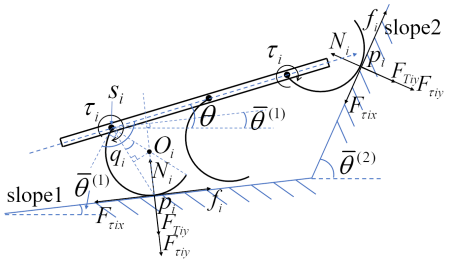

Fig. 6. Diagram of the forces at the ith touchpoint.

Transferring the torque of the hip joint $\tau_i\,(i = 1, \cdots, 6)$ to the touchpoint, we can get the force which is perpendicular to the arm S_iP_i, and its component in the coordinate system $O_{pi}X_{pi}Y_{pi}Z_{pi}$ can be described as

$$\begin{cases} F_{\tau ix} = \dfrac{\tau_i}{2l_r} \\ F_{\tau iy} = \dfrac{\tau_i}{2l_r}\tan\left(\dfrac{\pi - q_i + \theta - \bar{\theta}_i}{2}\right) \end{cases} \tag{3}$$

where $F_{\tau xi}$ and $F_{\tau yi}$ are the components of the O_pX_p axis and the O_pY_p axis, respectively, and $\bar{\theta}_i$ is the pitch angle of the wall on which the ith leg is located. Notably, although both $\bar{\theta}^{(k)}$ and $\bar{\theta}_i$ are the pitch angle of the wall, the difference between them is that $\bar{\theta}^{(k)}$ is the pitch angle of the kth wall, which is a wall-specific concept. However, when HUHR starts to transition, its front and rear legs will be on different walls, so $\bar{\theta}_i$ is introduced to denote the pitch angle of the wall on which the ith leg is located, which is a leg-specific concept. The value of $\bar{\theta}_i$ is taken as $\bar{\theta}^{(k)}$.

The vertical force F_{Tiy} required at the ith touchpoint is determined using the no-slip constraint, as shown in (4), which will provide sufficient positive pressure between the C-shape leg and the wall.

$$\begin{cases} |F_{\tau ix}| \leq \mu N_i \\ N_i = F_{Tiy} + F_{\tau iy} \end{cases} \tag{4}$$

where μ is the friction coefficient of the wall.

Based on the definition of the coordinate system, the rotation matrix ${}^{b}_{pi}\mathbf{R}$ from the touchpoint coordinate system to the body-fixed coordinate system can be described as

$${}^{b}_{pi}\mathbf{R} = \begin{bmatrix} \cos\left(\theta - \bar{\theta}_i\right) & \sin\left(\theta - \bar{\theta}_i\right) & 0 \\ -\sin\left(\theta - \bar{\theta}_i\right)\cos\varphi & \cos\left(\theta - \bar{\theta}_i\right)\cos\varphi & \sin\varphi \\ \sin\left(\theta - \bar{\theta}_i\right)\sin\varphi & -\cos\left(\theta - \bar{\theta}_i\right)\sin\varphi & \cos\varphi \end{bmatrix} \tag{5}$$

where φ, θ and ψ are the roll angle, the pitch angle and the yaw angle of HUHR, respectively.

Transferring F_{Tiy} to the center of mass of HUHR, we can obtain

$$\begin{bmatrix} T_x \\ T_y \\ T_z \end{bmatrix} = \sum_{i=1}^{6} a_i {}^{b}_{pi}\mathbf{R} \cdot \begin{bmatrix} 0 \\ F_{Tiy} \\ 0 \end{bmatrix} \tag{6}$$

where T_x, T_y, T_z denotes the force required at the center of mass of the robot, provided by thrusters. a_i denotes the touchdown state of the ith C-shape leg, where $a_i = 1$ means the C-shape leg touches the wall and $a_i = 0$ means the C-shape leg is off the wall.

Therefore, the control input of each thruster can be described as

$$\begin{bmatrix} T_1^b & \dots & T_8^b \end{bmatrix}^\top = \mathbf{C}_t^{-1} \begin{bmatrix} T_x & T_y & T_z & 0 & 0 & 0 \end{bmatrix}^\top \tag{7}$$

where $\mathbf{C}_t^{-1}$ is the pseudo-inverse of $\mathbf{C}_t$.

D. Gravity and Buoyancy

Since the center of buoyancy and gravity does not coincide, the gravity and buoyancy will generate restoring force and the restoring moment $\mathbf{g}(t)$, which can be described as

$$\mathbf{g}(t) = \begin{bmatrix} (B-G)\sin\theta \\ (B-G)\cos\theta\cos\varphi \\ -(B-G)\cos\theta\sin\varphi \\ B\cos\theta\left(y_c\sin\varphi + z_c\cos\varphi\right) \\ -B\left(x_c\cos\theta\sin\varphi + z_c\sin\theta\right) \\ B\left(y_c\sin\theta - x_c\cos\theta\cos\varphi\right) \end{bmatrix} \tag{8}$$

where B and G are the buoyancy and gravity of the robot, respectively, and B is slightly greater than G. $\mathbf{r}_B = \begin{bmatrix} x_b & y_b & z_b \end{bmatrix}^T$ is the coordinates of the center of buoyancy in the body-fixed coordinate system. In order to reduce the recovery moment, we set the center of buoyancy of HUHR close to the center of gravity.

E. Problem Formulation

The purpose of this paper is to design appropriate control input for HUHR, including the desired rotation angle q_i^d of each hip joint and the control input T_i of each thruster, so that the robot will be capable of continuous legged locomotion from a horizontal wall to a large-angled wall without slipping, as well as directional climbing.

III. Gait Planning and Control Methods

A. Transition Phase

When the front leg of HUHR touches the next wall and starts to transition, the position of leg 1 or leg 2 is shown in Fig. 7(a). Based on the single-leg kinematic model described above, when the robot moving on wall 1 with a tripod gait, the touchpoints corresponding to the angle of touchdown and off-wall are P and Q, respectively. When $q = \pi$, the touchpoint is M and SM is perpendicular to wall 1. However, if the robot keeps the original gait, its leg will come into contact with wall 2 during the swinging phase. Because the angular velocity of the hip joint during the swinging phase is too large, the robot will be subjected to too much force provided by the wall, which would cause the robot to slip too easily to climb the next wall or even fall over. Furthermore, if there are both legs in the swinging phase and supporting phase touch the wall, the robot will not be able to meet the tripod gait constraint, and these issues will prevent the robot from behaving decently.

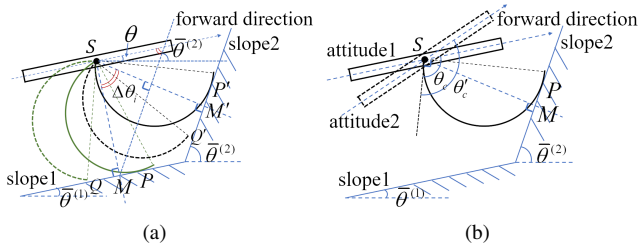

Fig. 7. (a) The movement of the C-shape leg. (b) Pitch angle of robot.

Therefore, in order to improve the stability and success rate of transition for HUHR, it is necessary to ensure that the C-shape leg rolls along the wall 2 in the supporting phase. As shown in Fig. 7(a), the touchpoints corresponding to the touchdown angle and off-wall angle should be adjusted to P' and Q', respectively. At the same time, when the leg rolls along the wall 2 up to the center of the supporting phase, the touchpoint is need to meet M' and SM' need to be perpendicular to the wall 2. In summary, the supporting phase is turned counterclockwise $\Delta\theta_i$ accordingly, which can be described as

$$\Delta\theta_i = \bar{\theta}_i - \theta \tag{9}$$

where $\bar{\theta}_i$ is the pitch angle of the wall where the ith touchdown leg is located, the value of $\bar{\theta}_i$ is $\bar{\theta}^{(1)}$ or $\bar{\theta}^{(2)}$.

As HUHR climbing up the wall 2, the movement of the robot is shown in Fig. 8. It can be seen that the pitch angle of the robot θ will gradually approach the angle of wall 2 $\bar{\theta}^{(2)}$, so $\Delta\theta_i$ will keep decreasing until to 0.

In addition, the pitch angle of HUHR will change during a gait period, as shown in Fig. 7(b). At the beginning of a gait period, the attitude of the robot is shown as "attitude1", and after a gait period, the robot changes to attitude 2, which is the

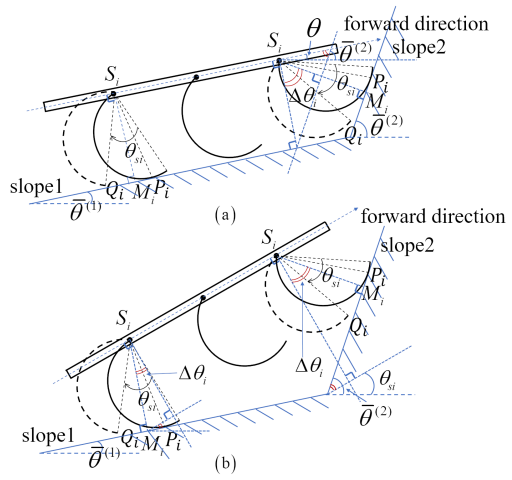

Fig. 8. The transition gait of HUHR.

initial attitude for the next gait period. Referring to TABLE I, θ_c and θ'_c are the touchdown angle for the current and next gait period, respectively. It is easy to know that $\theta'_c \neq \theta_c$ and the change of the touchdown angle is equal to the change of the robot's pitch angle. Therefore, with constant θ_{si}, because θ_c has changed, the swing angle θ_{ti} should be slightly greater than $2\pi - \theta_{si}$ to ensure that the swinging phase can alternate continuously with the next period-supporting phase. We use $k\Delta\theta_i$ to characterize the change of the robot's pitch angle, i.e. the change of swing angle, during one gait period, and $k > 0$ is a constant to be designed.

When the front leg (leg 1 or leg 2) of HUHR touches the wall 2, as shown in Fig. 9, the touchdown leg goes through a supporting phase and the body of the robot will move from position 1 to position 2, and each hip joint will move from $A/B/C$ to $A'/B'/C'$, respectively. a and b are the distance that the front and the rear hip joint moves along the walls, respectively. L is the distance between the front and the rear hip joints, the relationship between a and b can be described as

$$\begin{aligned} b &\approx L + |AD| - |C'D| \\ &= L + a\cos\left(\bar{\theta}^{(2)} - \bar{\theta}^{(1)}\right) - \sqrt{L^2 - \left(a\sin\left(\bar{\theta}^{(2)} - \bar{\theta}^{(1)}\right)\right)^2} \end{aligned} \tag{10}$$

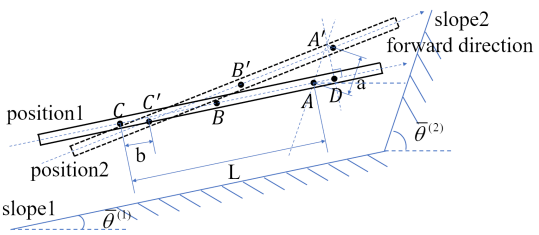

Fig. 9. The displacement of the hip joints.

Since HUHR is a rigid body, in the case of no slip, when the center of mass of the robot moves, the displacement of the front and rear hip joints will be unequal, which along the wall where they are located respectively. From (2), the displacement of hip joint is determined by the support angle. As a result, neglecting the undulation of the center of mass, the relationship between the support angle of the leg rolling along wall 1 $\theta_s^{(1)}$ and the leg rolling along wall 2 $\theta_s^{(2)}$ can be described as

$$\begin{aligned} &L + \left(\frac{\theta_s^{(2)}}{2} + 3\sin\frac{\theta_s^{(2)}}{2}\right) l_r \cos\left(\bar{\theta}^{(2)} - \bar{\theta}^{(1)}\right) \\ &- \sqrt{L^2 - \left(\left(\frac{\theta_s^{(2)}}{2} + 3\sin\frac{\theta_s^{(2)}}{2}\right) l_r \sin\left(\bar{\theta}^{(2)} - \bar{\theta}^{(1)}\right)\right)^2} \\ &\approx \left(\frac{\theta_s^{(1)}}{2} + 3\sin\frac{\theta_s^{(1)}}{2}\right) l_r \end{aligned} \tag{11}$$

According to [7], [10], each parameter of Hopf oscillator has clear physical meaning and can be adjust independently, so we use Hopf oscillator as the gait generator of HUHR, whose mathematical model can be described as

$$\dot{\mathbf{X}}_{\mathrm{i}} = \begin{bmatrix} \dot{u}_i \\ \dot{v}_i \end{bmatrix} = \begin{bmatrix} \sigma\left(R^2 - u_i^2 - v_i^2\right) u_i - 2\pi\omega v_i \\ \sigma\left(R^2 - u_i^2 - v_i^2\right) v_i + 2\pi\omega u_i \end{bmatrix} + \lambda \sum_j \Delta_i^j \tag{12}$$

where $\mathbf{X}_i = [u_i \quad v_i]^T$ is the state variable of the ith oscillator, i.e. the output signal of the oscillator. σ is the convergence factor, R is the limit ring radius, ω is the oscillation frequency, and λ is the coupling coefficient. Δ_i^j is the action of the jth oscillator on the ith oscillator in the CPG network, which can be described as

$$\Delta_i^j = \begin{bmatrix} \cos\phi_i^j & -\sin\phi_i^j \\ \sin\phi_i^j & \cos\phi_i^j \end{bmatrix} \begin{bmatrix} u_i \\ v_i \end{bmatrix} \tag{13}$$

where ϕ_i^j is the phase difference of the jth oscillator to the ith oscillator.

Since the output signal is similar to a sine function, we choose sine function for mapping. In summary, the relationship between the output signal of the ith Hopf oscillator and the desired rotation angle of the ith hip joint is mapped as

$$q_i^d\left(u_i\right) = \begin{cases} \dfrac{\theta_{si}}{2}\sin\left(\dfrac{\pi}{2}u_i\right) + \pi - \Delta\theta_i, \\ \qquad\qquad \text{if } (v_i \leq 0) \\ -\dfrac{\theta_{ti}}{2}\sin\left(\dfrac{\pi}{2}u_i\right) + \dfrac{\theta_{ti}}{2} + \dfrac{\theta_{si}}{2} + \pi - \Delta\theta_i, \\ \qquad\qquad \text{if } (v_i > 0) \end{cases} \tag{14}$$

where $\Delta\theta_i$ is the angle between the normal of the wall and the negative direction of the O_bY_b axis, θ_{si} is the support angle of the ith leg, taking the value of $\theta_s^{(1)}$ or $\theta_s^{(2)}$, θ_{ti} is the swing angle of the ith leg, satisfying $\theta_{ti} = 2\pi - \theta_{si} + k\Delta\theta_i$.

Using the tracking error, the torque of the ith joint can be solved with PD controller, and the control law is designed as

$$\tau_i = k_p\left(q_i^d - q_i\right) + k_d\left(\dot{q}_i^d - \dot{q}_i\right) \tag{15}$$

where k_p and k_d are the parameters of the proposed controller,

q_i and $\dot{q}_i$ are the true rotation angle and angular velocity of the ith leg, respectively.

In addition, because of using the tripod gait, during the transition phase, as shown in Fig. 8, the robot tends to "head up". As a result, only the front and rear legs on the same side will be in contact with two different walls, while the two middle legs are suspended, which causes the robot to lean to one side, creating a roll angle. In order to reduce the roll angle of the robot during the transition phase, the rolling moment can be designed as

$$M_{Tx} = -k_\varphi \varphi \tag{16}$$

where $k_\varphi > 0$ is a constant to be designed.

In summary, in order to ensure that the C-shape leg of HUHR does not slip and that the attitude of the robot does not fluctuate significantly, the control input of each thruster can be designed as

$$\begin{bmatrix} T_1 & \dots & T_8 \end{bmatrix}^\top = \mathbf{C}_t^{-1} \left(\begin{bmatrix} T_x & T_y & T_z & M_{Tx} & 0 & 0 \end{bmatrix}^\top - \mathbf{g}(t) \right) \tag{17}$$

where $T_i\,(i = 1, 2, \cdots, 8)$ is the control input of ith thruster. $T_x/T_y/T_z$ is the basic thrust under the no-slip constraint, which is calculated by (6). $\mathbf{g}(t)$ is calculated by (8). On this basis, since the friction coefficient in the water is difficult to obtain, we can set a basic thrust to T_3 and T_4 in order to ensure that the rear legs do not slip during transition phase.

B. Climbing Phase

For the climbing task, the tripod gait is still used, and the relationship between the output signal of the ith Hopf oscillator and the desired rotation angle of the ith hip joint is mapped as

$$q_i^d(u_i) = \begin{cases} \dfrac{\theta_{si}}{2} \sin\left(\dfrac{\pi}{2} u_i\right) + \pi, & \text{if } (v_i \le 0) \\ -\dfrac{\theta_{ti}}{2} \sin\left(\dfrac{\pi}{2} u_i\right) + \dfrac{\theta_{ti}}{2} + \dfrac{\theta_{si}}{2} + \pi, & \text{if } (v_i > 0) \end{cases} \tag{18}$$

Meanwhile, in order to achieve directional climbing, the tracking error of yaw angle is introduced into the calculation of support angle, which can be described as

$$\theta_{si} = k_\psi M(i)(\psi - \psi_d) + \theta_{s0} \tag{19}$$

where ψ_d is the desired yaw angle of HUHR. k_ψ is the parameter of the controller. θ_{s0} is the initial value of the support angle, $M(i)$ characterizes the left and right legs of the robot, which is defined as

$$M(i) = \begin{cases} 1, & i = 1, 3, 5 \\ -1, & i = 2, 4, 6 \end{cases} \tag{20}$$

In addition, the control input of each thruster during the climbing phase can be described as $T_i = T_i^b + T_i^a\,(i = 1, 2, \cdots, 8)$, where basic thrust $T_i^b\,(i = 1, 2, \cdots, 8)$ is calculated by (7) to ensure that the C-shape leg of the robot does not slip, additional thrust $T_i^a = -\mathbf{C}_t^{-1}\mathbf{g}(t)\,(i = 1, 2, \cdots, 8)$ is calculated by (8) to overcome the recovery force and recovery moment.

C. Algorithm Implementation

In this paper, as shown in Fig. 10, we design a gait planning and control method for wall climbing and transition of HUHR. Based on the forward distance(d) between the wall and the center of mass of the robot, as well as the pitch angle of the robot (θ) and the walls $(\bar{\theta}^{(k)})$, we set switch signals c_1 and c_1 shown in (21) to characterize the gait switching. If $c_1 = 1$, the transition phase will be start, if $c_2 = 1$, the transition phase will be over and the robot start to climb along the wall.

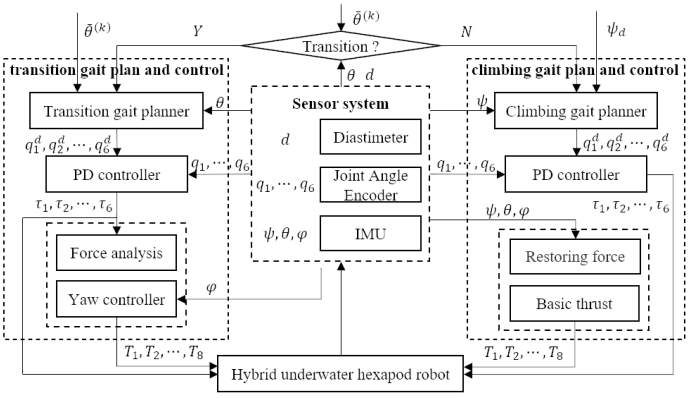

Fig. 10. Diagram of the gait planning and control methods.

$$c_1 = \begin{cases} 1, \text{if } (d \le D) \\ 0, \text{else} \end{cases} \quad c_2 = \begin{cases} 1, \text{if } \left(\left| \theta - \bar{\theta}^{(k)} \right| \le \vartheta \right) \\ 0, \text{else} \end{cases} \tag{21}$$

where D and ϑ are the threshold of the forward distance and angle error, respectively. c_1 characterizes the switch from climbing to transition, and c_2 is just the opposite.

IV. Experiments

A. Experiment Setting

As shown in Fig. 11, we carried out the experimental verification in a $3\text{m} \times 3\text{m} \times 10\text{m}$ pool, to verify that our robot is capable of continuous legged locomotion from a horizontal plane to a vertical plane. However, the experimental platform has no positioning system and distance measurement equipment. Therefore, we use sudden change of the robot's pitch angle to calculate the switch signals c_1 in (21), and we

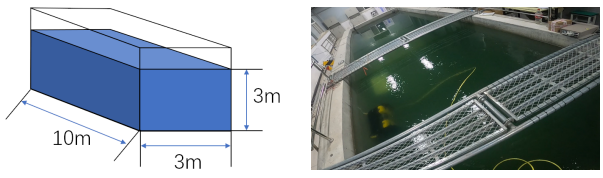

(a) (b)

Fig. 11. The experiment site.

use the integral of velocity to calculate the position of the robot over a short period of time. During the experiment, the errors of the sensors have no obvious influence on the behavior of the system, so this paper does not use any type of filtering measures.

The robot starts at $(x_0, y_0, z_0) = (0, 0, 0)$, the initial yaw angle is $\psi_0 = -1.08$rad, the desired yaw angle is $\psi_d = 0$rad. From the continuous legged locomotion from the horizontal plane to the vertical plane, we can obtain that $\bar{\theta}^{(1)} = 0$rad, $\bar{\theta}^{(2)} = \frac{\pi}{2}$rad. The initial support angle of the C-shape leg is $\theta_{s0} = 0.78$rad. The friction coefficient in the environment is $\mu = 0.6$, the basic thrust to T_3 and T_4 is 4N. The parameters of the proposed controller are chosen as $k = 0.2$, $k_\psi = 4$, $k_\varphi = 10$, $k_p = 10$, $k_d = 0$, the step size is set to 0.02s.

B. Experimental Results

Fig. 12 shows the movement of HUHR in the experiment, in which (a)-(f) is the transition phase and (g)-(i) is the climbing phase. Fig. 13 (a) shows the trajectory of HUHR in three-dimensional space, in which the angle of wall 2 is $\bar{\theta}^{(2)} = \frac{\pi}{2}$rad. Fig. 13 (b) shows the the trajectory of HUHR in the horizontal plane and the vertical plane. We observe that the robot gradually "lifts its head" and climbs up to the vertical plane. During the climbing phase, the robot is able to climb along wall 2, climbing along the O_0Y_0 axis for 1.8 m.

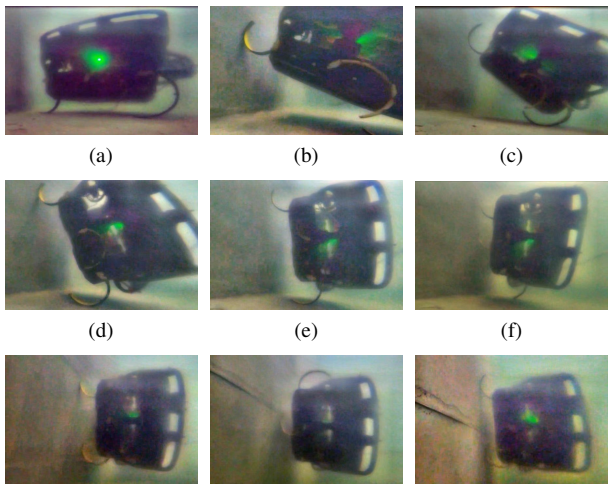

Fig. 12. The movement of HUHR in the experiment.

Fig. 14 shows the yaw angle and pitch angle of HUHR, in which the yaw is chattering around the desired value and the pitch is varying with the angle of the wall. The tracking error of the yaw angle can converge to ± 0.2rad. The reason for the yaw angle tracking error is the complexity of hydrodynamic force and underwater friction coefficient, maybe coefficient of friction is unlikely to be a constant. We can alse observe that the transition phase started at t=34s and lasted 6s. It's worth noting that it might take a little while for the robot to notice that it has hit a vertical wall. Because we use sudden change of pitch angle instead of the switch signals c_1 in (21), but in fact, when the robot touches the vertical wall with original

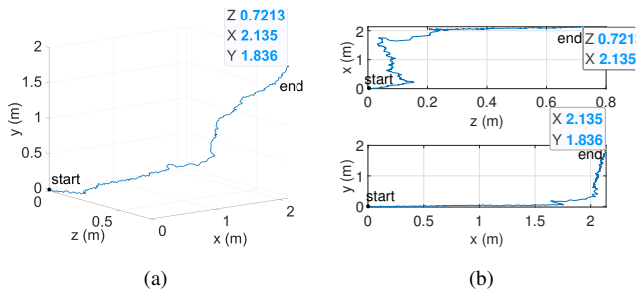

Fig. 13. Trajectory of HUHR. (a) Trajectory in three-dimensional space. (b) Trajectory in the horizontal plane and the vertical plane.

gait, the pitch angle of the robot does not necessarily change dramatically right away.

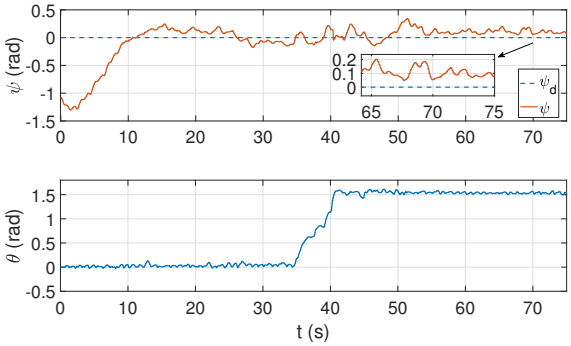

Fig. 14. Yaw angle and pitch angle of HUHR.

In Fig. 15 and Fig. 16, the desired rotation angle of each hip joint and the control input of each thruster are presented, respectively. As shown in Fig. 15, during the transition phase, i.e., $t = 34\text{s} \sim 40\text{s}$, for leg 5 or leg 6 which rolls along wall 1, $\Delta\theta_i = 0 - \theta < 0$, so θ_c and θ_f increase. For leg 1 or leg 2 which rolls along wall 2, $\Delta\theta_i = \bar{\theta}_i - \theta > 0$, so θ_c and θ_f will decrease. The experimental results are consistent with the theoretical analysis. As shown in Fig. 16, during the transition phase, as the pitch angle and the gait of HUHR change significantly, the control input of each thruster fluctuates significantly, and both vertical and lateral thrusters are used to provide positive pressure on the leg. After $t = 40$s, the robot climbs up the wall 2 and its pitch angle remains stable, so the control input is essentially stable and positive pressure on the leg is provided only by the vertical thrusters, at which point the vertical thrusters generate a positive pitch moment, preventing the pitch angle of the robot from decreasing.

During the transition phase, the attitude of HUHR slightly fluctuates, which is due to the fact that the effects of hydrodynamics were not considered when performing the no-slip constraint analysis. However, the inertia of the robot, the damping of the water, and the ocean currents all affect the stability of the robot. Therefore, we will consider the effects of hydrodynamics and ocean currents for further study, and make legged locomotion smoother.

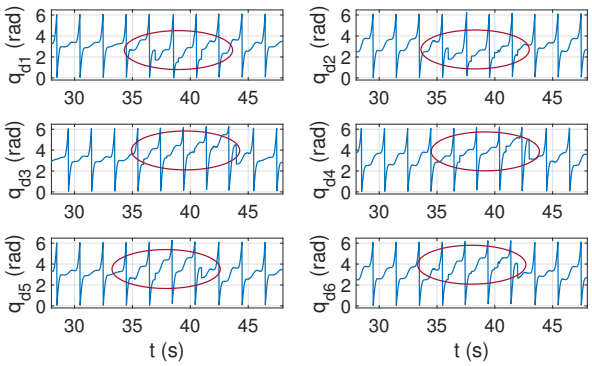

Fig. 15. The desired rotation angle of hip joints in the experiment.

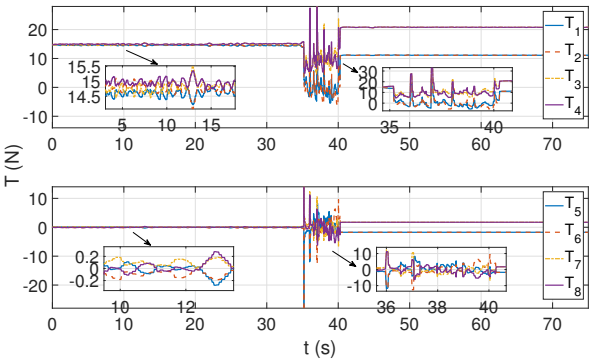

Fig. 16. Control inputs for eight thrusters in the experiment.

V. Conclusion

In this paper, we have proposed a motion planning method for HUHR, which let the robot become capable of continuous legged locomotion from a horizontal wall to a large-angled wall, as well as directional climbing. The stable walking constraint of the C-shape leg is analyzed, and the control input of each thruster adapted to the torque of the hip joints is solved. On this basis, by introducing the pitch angle of the robot and the pitch angle of the plane, an aperiodic mapping from the output of the Hopf oscillator to the desired rotation angle of the hip joint is designed. Meanwhile, the stability and adaptiveness of the climbing motion are improved. Furthermore, the effectiveness of the proposed method has been verified on HUHR.

References

[1] M. Garcia, A. Chatterjee, and A. Ruina, "Efficiency, speed, and scaling of two-dimensional passive-dynamic walking," *Dynamics and Stability of Systems*, vol. 15, no. 2, pp. 75–99, 2000.

[2] U. Saranli, M. Buehler, and D. E. Koditschek, "Rhex: A simple and highly mobile hexapod robot," *The International Journal of Robotics Research*, vol. 20, no. 7, pp. 616–631, 2001.

[3] C. Li, P. B. Umbanhowar, H. Komsuoglu, D. E. Koditschek, and D. I. Goldman, "Sensitive dependence of the motion of a legged robot on granular media," *Proceedings of the National Academy of Sciences*, vol. 106, no. 9, pp. 3029–3034, 2009.

[4] S. Zhang, X. Liang, L. Xu, and M. Xu, "Initial development of a novel amphibious robot with transformable fin-leg composite propulsion mechanisms," *Journal of Bionic Engineering*, vol. 10, no. 4, pp. 434–445, 2013.

[5] Y. Chou, K. Huang, W. Yu, and P. Lin, "Model-based development of leaping in a hexapod robot," *IEEE Transactions on Robotics*, vol. 31, no. 1, pp. 40–54, 2015.

[6] M. Harper, J. Pace, N. Gupta, C. Ordonez, and E. Collins Jr, "Kinematic modeling of a rhex-type robot using a neural network," in *Unmanned Systems Technology XIX*. International Society for Optics and Photonics, 2017, pp. 1–9.

[7] J. Yu, M. Tan, J. Chen, and J. Zhang, "A survey on cpg-inspired control models and system implementation," *IEEE Transactions on Neural Networks and Learning Systems*, vol. 25, no. 3, pp. 441–456, 2014.

[8] S. Zhang, Y. Zhou, M. Xu, X. Liang, J. Liu, and J. Yang, "Amphihex-i: locomotory performance in amphibious environments with specially designed transformable flipper legs," *IEEE/ASME Transactions On Mechatronics*, vol. 21, no. 3, pp. 1720–1731, 2015.

[9] H. Yu, H. Gao, L. Ding, M. Li, Z. Deng, and G. Liu, "Gait generation with smooth transition using cpg-based locomotion control for hexapod walking robot," *IEEE Transactions on Industrial Electronics*, vol. 63, no. 9, pp. 5488–5500, 2016.

[10] L. Bai, H. Hu, X. Chen, Y. Sun, C. Ma, and Y. Zhong, "Cpg-based gait generation of the curved-leg hexapod robot with smooth gait transition," *Sensors*, vol. 19, no. 17, pp. 1–26, 2019.

[11] G. Zhong, L. Chen, Z. Jiao, J. Li, and H. Deng, "Locomotion control and gait planning of a novel hexapod robot using biomimetic neurons," *IEEE Transactions on Control Systems Technology*, vol. 26, no. 2, pp. 624–636, 2017.

[12] S. Hachicha, C. Zaoui, H. Dallagi, S. Nejim, and A. Maalej, "Innovative design of an underwater cleaning robot with a two arm manipulator for hull cleaning," *Ocean Engineering*, vol. 181, pp. 303–313, 2019.

[13] H. Albitar, A. Ananiev, and I. Kalaykov, "New concept of in-water surface cleaning robot," in *2013 IEEE International Conference on Mechatronics and Automation*. IEEE, 2013, pp. 1582–1587.

[14] T. Guo, Z. Deng, X. Liu, D. Song, and H. Yang, "Development of a new hull adsorptive underwater climbing robot using the bernoulli negative pressure effect," *Ocean Engineering*, vol. 243, pp. 1–15, 2022.

[15] M. Malley, M. Rubenstein, and R. Nagpal, "Flippy: A soft, autonomous climber with simple sensing and control," in *IEEE/RSJ International Conference on Intelligent Robots and Systems (IROS)*, 2017, pp. 6533–6540.

[16] W. Huang, Z. Xu, J. Xiao, W. Hu, H. Huang, and F. Zhou, "Multimodal soft robot for complex environments using bionic omnidirectional bending actuator," *IEEE Access*, vol. 8, pp. 193 827–193 844, 2020.

[17] Y. Zhang, L. Ge, J. Zou, H. Xu, and G. Gu, "A multimodal soft crawling-climbing robot with the controllable horizontal plane to slope transition*," in *IEEE/RSJ International Conference on Intelligent Robots and Systems (IROS)*, 2019, pp. 3343–3348.

[18] Y. Zhang, D. Yang, P. Yan, P. Zhou, J. Zou, and G. Gu, "Inchworm inspired multimodal soft robots with crawling, climbing, and transitioning locomotion," *IEEE Transactions on Robotics*, 2021, doi:10.1109/TRO.2021.3115257.

[19] C. Park, J. Bae, S. Ryu, J. Lee, and T. Seo, "R-track: Separable modular climbing robot design for wall-to-wall transition," *IEEE Robotics and Automation Letters*, vol. 6, no. 2, pp. 1036–1042, 2021.

[20] H. Hariri, D. Koh, H. Lim, A. Dharmawan, V. Nguyen, G. Soh, S. Foong, R. Bouffanais, H. Low, and K. Wood, "Orion-ii: A miniature climbing robot with bilayer compliant tape for autonomous intelligent surveillance and reconnaissance," in *15th International Conference on Control, Automation, Robotics and Vision (ICARCV)*, 2018, pp. 1621–1626.

[21] D. Koh, A. Dharmawan, H. Hariri, G. Soh, S. Foong, R. Bouffanais, H. Low, and K. Wood, "Design and analysis of a miniature two-wheg climbing robot with robust internal and external transitioning capabilities," in *International Conference on Robotics and Automation (ICRA)*, 2019, pp. 9740–9746.

[22] K. Daltorio, T. Witushynsky, G. Wile, L. Palmer, A. Malek, M. Ahmad, L. Southard, S. Gorb, R. Ritzmann, and R. Quinn, "A body joint improves vertical to horizontal transitions of a wall-climbing robot," in *IEEE International Conference on Robotics and Automation*, 2008, pp. 3046–3051.

[23] G. Lee, H. Kim, K. Seo, J. Kim, and H. Kim, "Multitrack: A multi-linked track robot with suction adhesion for climbing and transition," *Robotics and Autonomous Systems*, vol. 72, pp. 207–216, 2015.

[24] T. Chen, Y. Li, X. Rong, and L. Zhou, "Realization of complex terrain and disturbance adaptation for hydraulic quadruped robot under flying trot gait," in *IEEE International Conference on Robotics and Biomimetics (ROBIO)*, 2019, pp. 2055–2060.